The Astronomical Journal, 166:68 (13pp), 2023 August https://doi.org/10.3847/1538-3881/ace25f

Newly Discovered Wolf–Rayet Stars in M31

Kathryn F. Neugent[1,4] and Philip Massey[2,3]
[1] Center for Astrophysics, Harvard & Smithsonian, 60 Garden Street, Cambridge, MA 02138, USA; Kathryn.Neugent@cfa.harvard.edu
[2] Lowell Observatory, 1400 W Mars Hill Road, Flagstaff, AZ 86001, USA
[3] Department of Astronomy and Planetary Science, Northern Arizona University, Flagstaff, AZ 86011-6010, USA
Received 2023 May 31; revised 2023 June 20; accepted 2023 June 20; published 2023 July 18

Abstract

The evolved massive star populations of the Local Group galaxies are generally thought to be well understood. However, recent work has suggested that the Wolf–Rayet (WR) content of M31 may have been underestimated. We therefore began a pilot project to search for new WRs in M31 and to reexamine the completeness of our previous WR survey, finished almost a decade prior. Our improved imaging data and spectroscopic follow-up confirmed 19 new WRs across three small fields in M31. These newly discovered WRs are generally fainter than the previously known sample due to slightly increased reddening as opposed to intrinsic faintness. From these findings, we estimate that there are another ∼60 WRs left to be discovered in M31; however, the overall ratio of WN-type (nitrogen-rich) to WC-type (carbon-rich) WRs remains unchanged with our latest additions to the M31 WR census. We are in the process of extending this pilot WR survey to include the rest of M31, and a more complete population will be detailed in our future work.

Unified Astronomy Thesaurus concepts: Wolf-Rayet stars (1806); Massive stars (732); Evolved stars (481); Andromeda Galaxy (39); Stellar populations (1622)

Supporting material: data behind figure, machine-readable tables

1. Introduction

Wolf–Rayet stars (WRs) are descended from the most massive of stars (>30 $M_{\odot}$) and are characterized by strong stellar winds that produce broad emission lines in their spectra (e.g., Cassinelli & Hartmann 1975; Conti 1978). WN-type, or nitrogen-rich WRs show emission lines of helium and nitrogen, the products of CNO-cycle hydrogen burning. WRs that have undergone even more stripping, through enhanced stellar winds or binary interaction, will instead show the helium-burning products of carbon and oxygen (WC type or WO type). Once these massive stars end their stellar lives, they leave behind black holes. Around 30%–40% of WRs exist in short-period (<10 day) binary systems (Bartzakos et al. 2001; Foellmi et al. 2003; Schnurr et al. 2008; Neugent & Massey 2014; Dsilva et al. 2022) and are the progenitors to the black hole mergers being detected as gravitational-wave events (Abbott et al. 2016). However, while constraints have been placed on the binary fraction of the short-period WR systems, the overall influence of binarity on the evolution of WRs, and massive stars in general, is still an open question.

To understand the relative importance of binarity on the evolution of WRs, we first must identify a complete population of them in nearby environments, such as in the star-forming galaxies of the Local Group. Luckily for us, WRs are relatively straightforward to identify observationally due to their characteristic strong and broad spectroscopic emission lines. Historically, our lack of knowledge about the WR populations within the Local Group was limited primarily due to observational resources rather than an inability to differentiate WRs from other stellar objects; see discussion in Massey & Johnson (1998), Neugent & Massey (2011), and Neugent et al. (2012). Within the last few decades, we have led several targeted surveys to identify populations of WRs within the Local Group galaxies of M31, M33, and the Magellanic Clouds (Neugent & Massey 2011; Neugent et al. 2012; Massey et al. 2014, 2015, 2017; Neugent et al. 2018) with reported completeness rates to within ∼5% or better. These surveys allow for exciting science to be done on galaxy-wide populations such as determining the physical and evolutionary properties of these stars (Hainich et al. 2015; Shenar et al. 2016, 2020), understanding how WR populations relate to expected supernovae and black hole production rates (Woosley et al. 2020; S. K. Sarbadhicary et al. 2023, in preparation), and investigating the impact of binary evolution by comparing the relative number of different types of massive stars across varying environments (Dorn-Wallenstein & Levesque 2018; Massey et al. 2021a).

In Massey et al. (2021a), we examined how the relative number of WRs and red supergiants (RSGs) should change as a function of metallicity and initial binary fraction within the Local Group. As is shown in Figure 11 of Massey et al. (2021a), we found generally good agreement between our observed WR/RSG ratio and model predictions from the Binary Population and Spectral Synthesis models (Eldridge et al. 2017) for all galaxies except in M31, where the models suggest an initial binary fraction of 0% (see additional discussion in Section 4 of Massey et al. 2021a). This result would be surprising, but is currently not ruled out observationally. However, a more reasonable question might be: Are we missing WRs in M31? This was not the first time we (and others) had pondered this question. Shara et al. (2016) found a reddened WR in M31 while searching for symbiotic stars and suggested that a "modest number of reddened WR stars remain to be found in M31." At the time, we (incorrectly) assumed that the star discovered by Shara et al. (2016) had

[4] NASA Hubble Fellow.

simply fallen in one of the chip gaps in our initial M31 study (Neugent et al. 2012) and concluded that this missing star was included in the 5% completeness error. However, the discovery by Shara et al. (2016) and the conclusions found by Massey et al. (2021a) motivated us to reinvestigate the WR population of M31.

Here, we present the results of this observational survey for additional WRs in M31. In Section 2, we identify the candidate WRs with interference filter imaging and image subtraction before obtaining their spectra. In Section 3, we give an overview of our new discoveries before discussing the broader implications of our survey's completeness in Section 4. Finally, we summarize our findings and offer concluding remarks in Section 5. Further information about our individual discoveries can be found in the Appendix.

2. Identifying New Wolf–Rayet Stars in M31

Strong emission lines make WRs easily identifiable using narrowband interference filter imaging. This method has been successfully used by us and others (e.g., Wray & Corso 1972; Moffat & Shara 1983; Armandroff & Massey 1985) and is discussed extensively in Neugent & Massey (2011). Here, we summarize our procedure of using interference filters on the 4.3 m Lowell Discovery Telescope (LDT) to identify candidate WRs in M31 before spectroscopically confirming them using Binospec on the 6.5 m MMT.

2.1. Candidate Identification with Interference Filter Imaging

Following the methods used successfully in our initial M31 survey (Neugent et al. 2012), we employed three interference filters optimized for the detection of WRs to be used on the LDT's Large Monolithic Imager (LMI). One filter is centered on the strongest emission line in WN-type WRs (*WN*; He II λ4686), one is centered on the strongest line in WC-type WRs (*WC*; C III/IV λ4650), and one is centered on neighboring continuum (*CT*; λ4750). The filter bandpasses are all 50 Å wide (FWHM). Physically the filters are 120 × 120 mm to avoid vignetting the $f/6$ beam.[5] Objects that are brighter in the *WC* or *WN* filters compared to in the continuum are considered viable WR candidates worthy of potential spectroscopic follow-up.

Our previous galaxy-wide interference imaging survey for WRs in M31 was conducted on the 4 m Mayall telescope at the Kitt Peak National Observatory (KPNO). The Mosaic CCD had a much larger field of view compared to that of LMI on the LDT ($36' \times 36'$ versus $12.'3 \times 12.'3$) and we were able to image the entire optical disk of M31 (2.2 deg^2) in 10 overlapping fields. Due to LMI's smaller field of view, we could not cover the same survey area in one observing season. Instead, we opted to image three fields with a higher signal-to-noise ratio (S/N) than what was obtained during the first survey, with the goal of both finding new WRs as well as quantifying the known shortcomings in our previous survey.

There were two issues with the previous Mosaic survey done by Neugent et al. (2012) that we hoped to improve upon. The first was due to the gaps within the eight-chip Mosaic CCD. While the images were dithered in an attempt to fill in the chip gaps, and the individual fields overlapped spatially, there were still regions missed. Additionally, poor cosmic-ray removal in the dithered regions hindered WR identification during the image-subtraction process. As discussed in Neugent et al. (2012), we complemented our image-subtraction techniques with photometry to identify stars that changed in magnitude between the on-band (*WC* and *WN*) and off-band (*CT*) images. The overall incompleteness due to gaps and cosmetics was estimated to be ∼5% by Neugent et al. (2012); here, we reexamine the issue in Section 4.

The second issue was that the survey suffered from poor and variable seeing. Ideally, variable seeing (and thus point-spread functions, PSFs) should not pose a problem for image-subtraction techniques due to the various cross-convolution methods employed. However, while completing a similar survey for WRs in the Magellanic Clouds (Massey et al. 2014, 2015, 2017; Neugent et al. 2018), we found that the maximum difference in seeing between images had to be less than $0.''2$ or else the image-subtraction routines lost effectiveness. Because this was not well understood during the original Mosaic M31 observations, and observing time was not in unlimited supply, the seeing fluctuations varied up to $0.''5$, leading to individual fields with poor image-subtraction results.

Putting these two shortcomings together, we opted to reimage regions of M31 that were plagued both by chip gaps and unstable seeing during the original survey. We additionally focused on areas of M31 with dense OB populations and a large number of known WRs. We also made sure to include the reddened WR discovered by Shara et al. (2016) in an attempt to better understand if our new observational setup would be able to detect it. The coordinates of our selected fields can be found in Table 1, and their locations within M31 relative to the known WRs are shown in Figure 1.

Table 1
Observation Summary

Name	Coordinates	Date Obs. (UT)	Seeing	Filter	Exp. Time (s)
Field 1	00:43:46.40 +41:46:11.3	2021 Sep 8	$0.''9$		
				WN	2 × 1200
				CT	2 × 1200
				WC	⋯
Field 2	00:44:25.00 +41:21:00.0	2021 Sept 9	$0.''8$		
				WN	2 × 1200
				CT	2 × 1200
				WC	900
Field 3	00:40:25.00 +40:39:27.0	2021 Oct 4	$0.''8$		
				WN	1200
				CT	1200
				WC	900

2.1.1. Observing and Image Reduction

We observed three regions of M31 with LMI on the 4.3 m LDT during dark time in Fall 2021. Our overall goal was to obtain multiple 20 minute exposures in each of the *WN*, *WC*, and *CT* filters and then produce final, combined images to identify candidate WRs using image subtraction and photometry. However, due to technical issues and variable seeing, we were not entirely successful. For all three fields, we managed to obtain at least one 20 minute image in the *WN* and *CT* filters with consistent seeing. In two fields we additionally

[5] The three filters were manufactured to our specifications by the Andover Corporation in September 2016, and have peak transmissions of ∼80%.

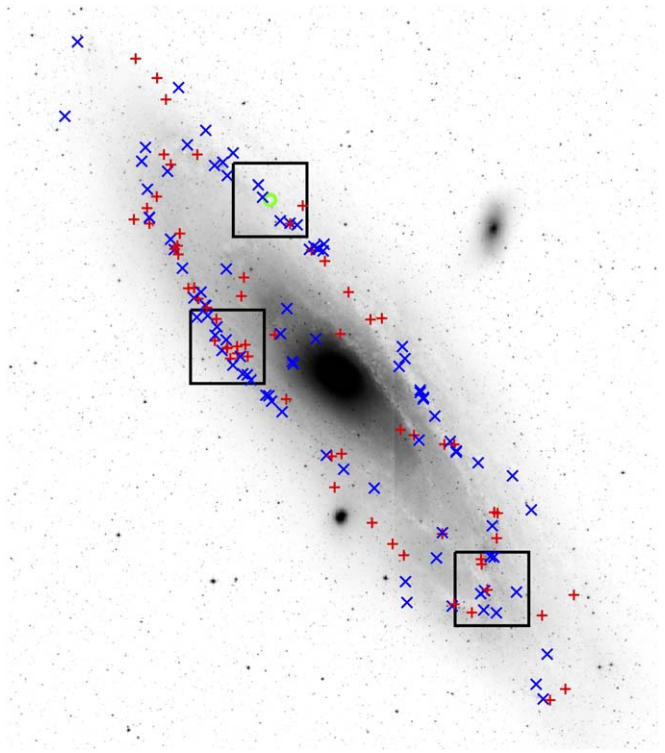

Figure 1. Locations of known WRs in M31 as well as new fields observed in this survey. The blue ×'s represent WN-type stars while the red +'s represent WC-type stars from Neugent et al. (2012). The green circle is the reddened WR discovered by Shara et al. (2016). The three fields observed in this survey with LMI are denoted by black boxes.

obtained a shorter *WC* image as well as additional 20 minute exposures with the *WN* and *CT* filters. While the lack of a *WC* image for Field 1 was disappointing, this did not hinder our ability to identify WR candidates; it just made it more difficult to differentiate them from planetary nebulae (PNe) before spectroscopic follow-up, as discussed below. A summary of our fields, dates observed, exposure times, and seeing conditions can be found in Table 1.

The LMI detector is a 92.2 mm by 92.4 mm single array of 6144 × 6160 e2v CCD231-C6 with a multilayer anti-reflective coating.[6] It is cooled to −120 °C using a Stirling closed-cycle cooler. Further details can be found in the instrument manual.[7] All images were taken with the detector binned by 2 × 2, resulting in a scale of $0\farcs24$ pixel^{-1}, and covering a field of view of $12\farcm3 \times 12\farcm3$. Although the detector has four excellent amplifiers, we chose to read our images out through a single one, simplifying the reduction process; in binned mode, the read-out time is only 24 s, small compared to our 20 minute exposure times. The read noise is 6e, and the gain is 2.9 e/ADU. The detector is operated at voltages in which it is linear to a fraction of a percent up to 150,000 e- and beyond.

Each image contains a 32-column overscan region, which was used to remove frame-to-frame dependent bias levels. There remains a significant bias structure, which we removed by averaging 10 bias frames, taken daily, although in practice the bias structure is stable on the timescale of months or even years. Multiple twilight flats were taken through each filter each evening with the telescope dithered between exposures to facilitate the removal of any stars bright enough to affect the flats. These exposures were averaged after scaling by their mode, and normalized by dividing by the median image value. Although the chip is otherwise excellent, there is a single bad column, which we ignored. All of these basic reductions took place using IRAF. A "pretty good" astrometric solution ($0\farcs3$) was added to each of the science images using the astrometry.net software (Lang et al. 2010).

2.1.2. Candidate Identification

To photometrically identify candidate WRs, we ran our own automated IRAF scripts to perform PSF-fitting photometry (based on DAOPHOT; see Stetson 1987). These scripts are adaptations for LMI of the programs used for the Local Group Galaxy Survey (LGGS) photometry described in Massey et al. (2006). Stars whose photometry was statistically significantly brighter in the on-band filter compared to the off-band filter were identified as potential WRs candidates, using the same methodology described in Neugent & Massey (2011) and Neugent et al. (2012). We emphasize that our photometry proved incidental to the discovery process, since many of the previously missed WRs were essentially invisible in the *CT* frame even in our new data, as described in the next section.

For image subtraction, we used the High Order Transform of PSF And Template Subtraction (HOTPANTS) code, written by Becker (2015). This allowed us to "subtract" the *CT* image from both the *WC* and *WN* images. Since WRs will have more flux in either the *WC* or *WN* images compared to in the *CT*, they will appear prominently in the subtracted image, as is shown in Figure 2. However, as is also shown in Figure 2, they are not the only stars that will show up in the subtracted images. Such contaminants are discussed below.

The three main non-WR contaminants that appear after image subtraction are saturated stars, red stars, and PNe. Saturated stars are relatively easy to discount as WR candidates because they are visually bright in all filters and the resulting image-subtracted "star" often has a noncircular shape (see star in the green box in Figure 2, for example). Red stars (generally foreground M dwarfs) appear as potential candidates because there is a TiO absorption line in the *CT* filter. This makes them appear brighter in the *WC* or *WN* filter compared to in the *CT*. While red stars were a large source of contamination in our first survey in M31 and M33 (Neugent & Massey 2011; Neugent et al. 2012), this time we cross-matched our candidates with the LGGS to identify stars with $B - V < 0.7$, as that corresponds to the color of a G-type dwarf and should remove the majority of any stars with TiO bands (Cox 2000). Finally, PNe additionally appear as potential WR candidates because they show He II λ4686 nebular emission if the radiation field is hard enough. The majority of PNe in M31 have been cataloged (e.g., Ciardullo et al. 1989; Merrett et al. 2006; Bhattacharya et al. 2019) and thus it was possible to cross-match our candidates with known PNe. Additionally, the fainter PNe tend to only show up through the *WN* filter (due to the nebular emission) and show nothing on the *CT* or *WC* image. However, since we were attempting to find reddened and faint WRs, we retained any such candidates until we could cross-match them with the PNe catalogs. In total, we removed 17 known PNe from our candidate list.

[6] Although this detector series is now in use at many other observatories, ours was the first of its kind. Some of the developmental engineering costs were supported by the purchase price and covered by a generous grant from the National Science Foundation through AST-1005313.

[7] http://www2.lowell.edu/users/massey/LMIdoc.pdf

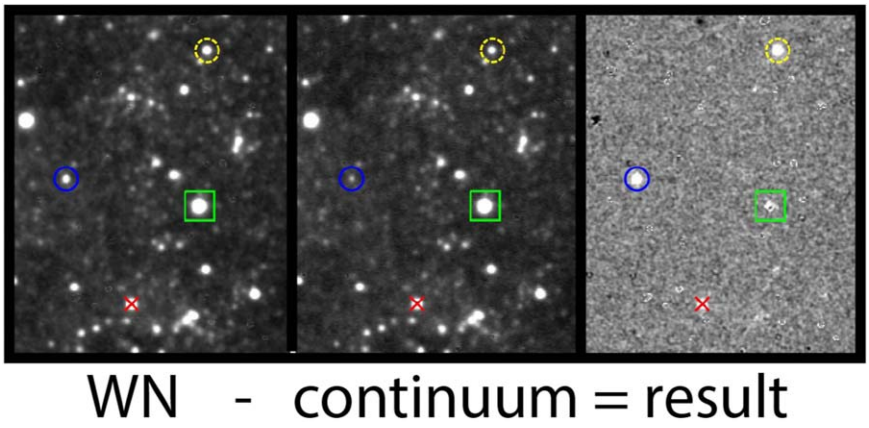

Figure 2. Using image subtraction to identify WR candidates. We used HOTPANTS (Becker 2015) to subtract the continuum image from the WN image to produce the final result. This particular region of the sky shows a previously known WR (yellow dashed circle), a saturated star that leads to a poor image-subtraction result (green box), a M-type star that shows up due to TiO absorption in the continuum filter (red ×), and a new WR candidate that was missed in our previous survey due to its faint magnitude (blue solid circle).

Using the subtracted images combined with the photometry, we created a list of potential WR candidates. After removing the various contaminates, we cross-matched our list with known WRs from Neugent et al. (2012). We successfully identified all of the known WRs in our three fields, which included 11 known WRs in Field 1, 19 in Field 2, and 8 in Field 3. Additionally, the WR discovered by Shara et al. (2016) showed up prominently on the *WN* field, but was too faint for detection in the *CT* image. After removing the known WRs, we were left with 30 new WR candidates. These 30 candidates were then divided into high, medium, and low priorities based on their likelihood of being a WR. There were 11 high-priority candidates that were detectable in both the *WN* and *WC* images (if available), as well as a weaker detection in the *CT*, and were thus likely not PNe. There were an additional 15 medium-priority candidates that had a strong detection in the *WN*, a weak detection in the *WC* (if available), but no detection in the *CT*. This led us to conclude that they were likely either newly found PNe or reddened WRs of WN-type, such as the one discovered by Shara et al. (2016, due to the weak detection in the *WC*). Finally, there were four remaining candidates that had very small photometric differences between the on- and off-band filters, but could potentially be Of-type stars and thus were still worth spectroscopically confirming.

After identifying our list of candidates with the LMI images, we needed better astrometry for the spectroscopic confirmation than the 0.″3 uncertainty that sufficed for the cross-identifications. Fortunately, LMI is often used for precise astrometry when determining the positions of asteroids and Kuiper Belt objects for recovery or orbital stability studies (e.g., Santana-Ros et al. 2022), or for orbital refinements in order to predict occultation tracks accurately (e.g., Levine et al. 2021)—both far more demanding tasks than ours. To facilitate such studies, care was taken in the design of the image corrector to minimize distortions that would affect the astrometry (Bida et al. 2012; DeGroff et al. 2014). The final astrometry of the WR candidates were determined using IDL routines written by Marc Buie,[8] with Gaia stars used as a reference (Gaia Collaboration et al. 2018, 2021). Transformations for each WN image were computed using ∼4500 Gaia stars using an 11th-order equation for the standard coordinates η and ξ with residual scatters of 0.″05.

[8] https://www.boulder.swri.edu/~buie/idl/

2.2. Spectroscopic Confirmation

To spectroscopically confirm the candidate WRs in M31, we used Binospec on the 6.5 m MMT located on Mt. Hopkins in southern Arizona (Fabricant et al. 2019). Its two 8′ × 15′ fields of view were a good match to our three LMI fields, and we were able to observe all 30 of our candidate WRs in three Binospec fields. They were observed during dark time on UT 2022 October 26 (Field 1), 2022 October 31 (first half of Field 2), 2022 December 14 (second half of Field 2), 2022 December 25 (first half of Field 3), and 2022 December 26 (second half of Field 3). The seeing ranged from 0.″9 to 2.″0, with the majority of the observations taken with a seeing of <1.″2, which was a reasonable match to our slit width of 1.″0. Fields 1 and 2 were observed with clear-sky conditions while Field 3 was observed with clouds. Exposure times were 3 hr long (broken up into 9 × 20 minute exposures) to achieve a S/N of 30 per 3.3 Å resolution element at ∼4500 Å, which we determined was adequate for classifying WRs in M31 in Neugent et al. (2012).

The optimal wavelength coverage to classify WRs is 4000 −5900 Å, which includes N IV λ4058, N V λλ4603, 19, N III λλ4634, 42, and He II λ4686 for WN types, and C III/IV λ4650, O V λ5592, C III λ5696, and C IV λ5806 for WC types. We opted to observe our candidates using the 270 l/mm grating, which gave us sufficient resolution, adequate sensitivity in the blue, and a ∼5400 Å wavelength range. Depending upon where a slit was located in the field, the wavelength shift could be as much as ±1300 Å, so we used a minimum central wavelength of 5501 Å to achieve as much coverage in the blue wavelength regime as possible. As a result, while the starting and ending wavelengths vary for each of the spectra, the minimum wavelength coverage ranges from 4020–7360 Å. The spectra were reduced on a night-by-night basis using the Binospec pipeline (Kansky et al. 2019). Due to variable quality, we chose not to combine spectra from multiple nights. Instead, we present the best versions in FITS format as "data behind figures" in the online journal, with the final exposure times for each spectrum available in the headers.

In an effort to fill the masks with targets, we additionally reobserved 22 known WRs in M31. A list of the known WRs we reobserved are in Table 2 with updated spectral types, as applicable. Additionally, these spectra are also available in FITS format as "data behind figures" in the online journal.

Table 2
Reobserved Known WRs

ID	Old Sp. Type[a]	New Sp. Type	Comments
J004020.44+404807.7	WC6	WC6	
J004022.43+405234.6	WC4	WC4	
J004023.02+404454.1	WN4	WN6	N III∼N IV; N V present but weak
J004026.23+404459.6	WN6+abs	WN6+abs	
J004031.67+403909.0	WN6	WN5-6	
J004034.17+404340.4	WC7+fgd	WC7+fgd	
J004034.69+404432.9	WC4	WC5?	Weak C III?
J004109.46+404907.8	WN6	WN6	
J004302.05+413746.7	WN9:	WN8	No N II
J004316.44+414512.4	WC6	WC7	
J004337.10+414237.1	Ofpe/WN9	Ofpe/WN9	
J004349.72+411243.4	WN6	WN6	
J004353.34+414638.9	WN7	WN6	
J004357.31+414846.2	WN8	WN8	
J004403.39+411518.8	WN6	WN4.5-5	
J004408.58+412121.2	WC6	WC6	
J004410.17+413253.1	WC6	WC6	
J004410.91+411623.2	WN4	WN4	
J004412.44+412941.7	WC6	WC6	
J004422.24+411858.4	WC7-8	WC7	
J004434.57+412424.4	WN3	WN4	N IV∼N V; N III absent
J004436.22+412257.3	WN5	WN6	

Note.
[a] Classifications from Neugent et al. (2012) and references therein.

(This table is available in machine-readable form.)

3. The Newly Discovered Wolf–Rayet Stars

Of the 30 WR candidates we identified, 19 are newly discovered WRs in M31. Of the remaining 11 candidates, one is an Of-type star with He II λ4686 emission (discussed more below), six are H II regions with nebular He II λ4686, three are cool stars with $B-V$ colors slightly below our red-color cutoff, and one is an A-type star that appeared as a candidate likely due to its brightness and resulting poor image subtraction. These stars are listed in Table 3 and are discussed individually in the Appendix. Additionally, spectra of a few representative WNs are shown in Figure 3 and WCs in Figure 4.

The WR classification criteria are nicely enumerated in Table 2 of van der Hucht (2001). These criteria are primarily qualitative since the various complexities surrounding WR winds (mass-loss rates, density and velocity profiles, etc.) dictate that two WRs with the same subtype may still have line fluxes that differ by large amounts. Other line ratios may also differ significantly. Therefore, while there are no WR spectral "standards," we can still strive for consistency across classifications. The digital versions of similarly classified WRs in M31 and M33 can be found in a tar file published as part of Neugent et al. (2012). Furthermore, digital optical spectra of most of the single Galactic WN stars described by Hamann et al. (1995) can be found here.[9] Finally, additional WN and WC stars from Torres-Dodgen & Massey (1988) can be downloaded from Vizier.

The spectral subtypes of WN stars are based upon the relative strengths of N III $\lambda\lambda$4634, 42, N IV λ4058, and N V $\lambda\lambda$4603, 19, with early types (such as WN3) assigned to stars where N V dominates, and later types (such as WN9) where N III dominates, with the strength of N III relative to He II λ4686 serving as a secondary criterion to distinguish the WN7 from the WN8 classes. The evolutionary connection between these classes is not clear owing to the disconnect between what is happening in the interior of these stars and the ionization balance in the outflowing wind where the emission lines are produced. Generally, the late-type WNs show the presence of hydrogen, while earlier types do not. (Hydrogen readily reveals itself as the even-n Pickering lines of He II are coincident with the Balmer lines. Both the He II and Balmer lines will show a decrease in strength going to shorter wavelengths, but if there is an odd/even pattern to the progression, with the even-n Pickering lines being stronger, that shows that hydrogen is still present; see Conti et al. 1983.)

Similarly, the WC subtypes are determined from the relative strengths of C IV $\lambda\lambda$5801, 12, C III λ5696, and O V $\lambda\lambda$5592. Again, the evolutionary connection between these ionization-based classifications is a topic of ongoing work; what is clear is that the WC stars are more chemically evolved than the WN stars. If O VI $\lambda\lambda$3811, 34 is present and *strong*, in some poorly defined sense, an early WC star is classified as a WO star. Recent work has shown that these WO stars are more evolved, with most of their helium converted to carbon and oxygen (Aadland et al. 2022). Finally, there are some WN stars that show abnormally strong C IV $\lambda\lambda$5801, 12. These are often referred to as "transition" stars, with the suggestion that they are WNs caught in the act of evolving to WCs, but the evidence here is also tenuous; see discussion in Hillier et al. (2021).

In terms of names, early studies of the M31 WR content used a hodgepodge of designations (see summary in Table 10 of Massey & Johnson 1998). All of the newly found WRs by Neugent et al. (2012), as well as the previously known ones, were in the LGGS, and they adopted these coordinate-based designations. The exceptions were two WC6 stars that were not

[9] https://www.astro.physik.uni-potsdam.de/~www/research/abstracts/wn-atlas_abstract.html

Table 3
Spectroscopic Results of New WR Candidates

Designation	R.A.	Decl.	EW[a]	FWHM[a]	Classification
J004019.66+404232.5	00:40:19.630	+40:42:32.40	−100	28	WN3
J004031.21+404128.1	00:40:31.190	+40:41:28.04	−130	18	WN7
X004032.57+403901.3	00:40:32.566	+40:39:01.30	−40	50	WC6+OB
J004039.59+404449.5	00:40:39.574	+40:44:49.42	−80	27	WN3
J004042.44+404505.3	00:40:42.423	+40:45:05.28	−100	23	WN4.5
X004045.57+404526.4	00:40:45.567	+40:45:26.42	⋯	⋯	⋯
X004054.05+403708.3	00:40:54.047	+40:37:08.29	−900	50	WC6
X004318.88+414711.1	00:43:18.876	+41:47:11.08	⋯	4.1	H II region
X004320.88+414107.0	00:43:20.884	+41:41:07.02	⋯	⋯	K7-M0
J004326.06+414260.0	00:43:26.022	+41:42:59.85	−130	46	WN4
X004332.04+414817.2	00:43:32.036	+41:48:17.16	⋯	4.6	H II region
X004338.95+414327.0	00:43:38.947	+41:43:26.98	⋯	26:	WN
X004341.15+414413.6	00:43:41.148	+41:44:13.65	−25:	20:	WN8/C
X004353.03+412141.0	00:43:53.032	+41:21:41.03	−75	17	WC
X004359.44+414823.9	00:43:59.439	+41:48:23.87	−30	25	WN6
J004404.10+411710.5	00:44:04.101	+41:17:10.37	⋯	⋯	H II region
X004406.41+412020.8	00:44:06.409	+41:20:20.78	−150	25	WN4.5
J004408.13+412100.6	00:44:08.113	+41:21:00.56	−48	20	WN4.5
J004413.56+412004.7	00:44:13.555	+41:20:04.46	−49	30	WN4.5
X004414.71+414033.3	00:44:14.708	+41:40:33.32	⋯	4.0	Symbiotic?
X004418.10+411850.8	00:44:18.101	+41:18:50.76	−190	90	WO
X004421.30+411807.2	00:44:21.301	+41:18:07.16	−4	20	O6 If
X004423.98+412255.6	00:44:23.981	+41:22:55.57	⋯	⋯	M2 I
X004425.09+412046.4	00:44:25.085	+41:20:46.44	−95	65	WC6+O8
X004426.99+411928.0	00:44:26.987	+41:19:28.03	⋯	⋯	A-type?
X004431.39+412114.0	00:44:31.393	+41:21:14.04	−175	35	WN3
X004432.06+411940.5	00:44:32.059	+41:19:40.46	⋯	⋯	H II region.
J004433.91+412501.2	00:44:33.903	+41:25:01.13	−65	22	WN6
X004438.04+412518.7	00:44:38.038	+41:25:18.73	−45	16	WN6
X004440.49+412052.1	00:44:40.486	+41:20:52.11	⋯	4.3	H II region

Note.
[a] Equivalent width (EW) and FWHM, both in units of angstroms, for He II λ4686 for WN stars, and C III/IV λ4650 for WC stars.
(This table is available in machine-readable form.)

in the LGGS. For these, Neugent et al. (2012) used LGGS-like designations but with an "X" instead of a "J" to avoid confusion. SIMBAD lists these as "[NMG2012] X J004256.05 +413543.7" and "[NMG2012] X J004308.25+413736.3," defeating our effort at simplification. Of our 20 newly found interesting stars, only eight appear in the LGGS, and thus we continue the "X" nomenclature here.

In Table 3, we include accurate coordinates and, when available, the LGGS designations. Note that there is a small offset between the given coordinates and the LGGS names. The LGGS names were tied to the USNO-B coordinates, while the coordinates of our newly found stars are on the ICRS, via Gaia, as described above. We also give the approximate equivalent widths of He II λ4686 (WN stars) or C III/IV λ4650 (WC stars), along with their FWHM line widths. For comparison, the H II regions in our sample have FWHMs of 4.5 Å at similar wavelengths, consistent with the expected resolving power of $R \sim 1340$.

4. Discussion

The confirmation of 19 newly discovered M31 WRs from our three LMI fields raises a number of important questions. Why were these new WRs missed as part of our previous, galaxy-wide survey with the Mosaic camera (Neugent et al. 2012)? Were they missed because they fell on the inter-chip gaps of the Mosaic camera, or are they fainter and required a higher sensitivity to be detected? If they are fainter, is this because the new WRs are *intrinsically* fainter, or are they simply more heavily reddened? And, finally, is this new survey deep enough, or if we increased our survey sensitivity would we simply keep finding more and more WRs? We must answer these questions quantitatively before estimating the total number of missing WRs in M31. Finally, as is discussed at the end of this section, the discovery of additional WRs in M31 raises the question of whether or not our complementary Mosaic survey in M33 (Neugent & Massey 2011) is also incomplete.

4.1. Why Were the Previous Wolf–Rayet Stars Missed?

We begin by addressing the first of these questions: Why were these 19 M31 WRs missed by Neugent et al. (2012)? The Kitt Peak Mosaic Camera used in that study consisted of eight 2K × 4K CCDs, with gaps between the chips. Each field was surveyed by obtaining nine exposures, three through each of the three narrowband filters (*WN*, *WC*, and *CT*) with the telescope offset (dithered) between exposures to help fill in the gaps. For each exposure, the gaps (and bad columns) affected, on average, ∼5% of the $36' \times 36'$ area covered by the exposure. The dithering process resulted in decreased sensitivity in 3 times this area when the data were combined. Thus, the affected area is ∼15%. This is ameliorated by the large overlap between adjacent fields. When we do a careful accounting, we expect about 9% of the survey area was affected. However, we likely did not lose *all* WRs within this

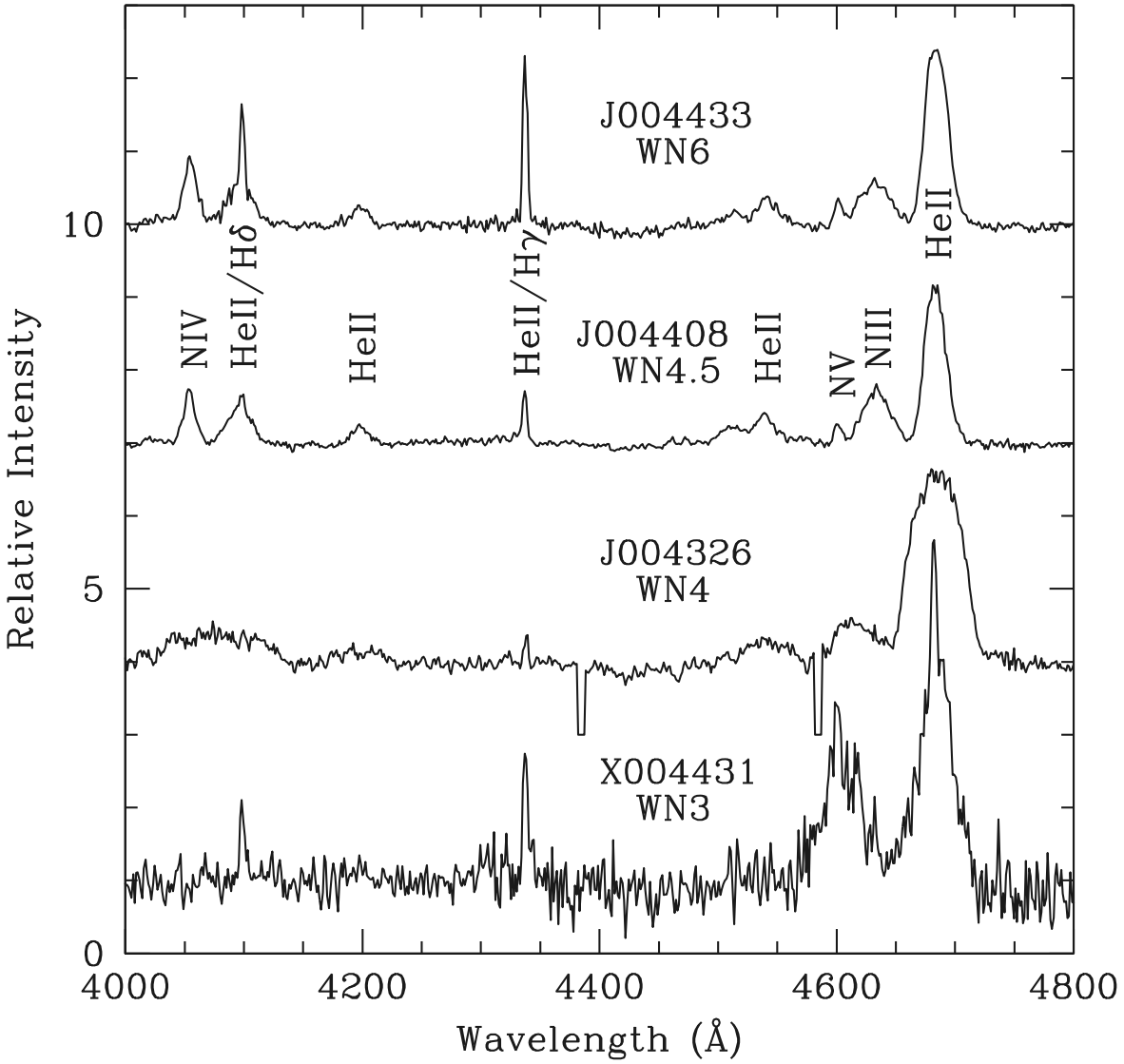

Figure 3. Spectra of representative WNs. We show four example spectra of newly found WN-type stars in M31. The spectra have been normalized, and only a portion of our wavelength coverage is shown for clarity. Each spectrum is offset from the previous by a relative intensity of 3.0. Lines identified include N IV λ4058, the He II/Hδ blend (contaminated by nebular emission in X004431.39+412114.0 and J004433.91+412501.2), He II λ4200, the He II/Hγ blend (with similar nebular contamination), He II λ4542, and the N V $\lambda\lambda$4603, 19 and N III λ4634, 42 doublets, as well as He II λ4686. Note that the unnormalized version of these, and all of our spectra, are being made available in FITS format as part of this publication as "data behind figures."

(The data used to create this figure are available.)

9%, as the gaps are *partially* filled in thanks to the dithering. Additionally, WRs with large differences between the on- and off-band magnitudes were detectable photometrically even in these dithered regions. Neugent et al. (2012) estimate an incompleteness of about 5% due to the gaps and other cosmetics, and our reevaluation here confirms that this is a reasonable estimate, with the incompleteness being preferentially biased toward the fainter WRs.

When we examine the location of the newly confirmed WRs on our old Mosaic data, we find that three fell into gaps, namely, J004031.21+404128.1, J004326.06+414260.0, and J004413.56+412004.7. We note that 39 of the previously known WRs fall on the LMI fields; thus, having missed three stars due to gaps is in reasonable accord with our expectations of 5%–10%. An additional new WR, X004425.09+412046.4, was missed due to crowding. The other 15 new WRs were missed as part of the previous survey because they were either very faint or invisible on the Mosaic images. Thus, the vast majority ($\sim$80%) of the newly found WR stars were not found in our earlier survey to a lack of sensitivity. However, this raises a new question: Are these new WRs intrinsically fainter than the previously known population of M31 WRs, or is their faintness caused by increased reddening?

To investigate whether these new WRs are intrinsically fainter than the previously known M31 WRs, we can compare their subtype distributions and inferred absolute magnitudes. In general, WN-type WRs are more difficult to detect than WC-type WRs due to weaker emission line fluxes (see, e.g., Conti & Massey 1989 and Massey & Johnson 1998), so we focus on the WN-type WRs for this comparison. Figure 5 shows the relative proportion of WN subtypes for both the previously known WNs in M31 ($N = 90$) as well as for the newly discovered sample of faint WNs ($N = 11$) due to removing the WCs and brighter WNs missed due to being in the Mosaic

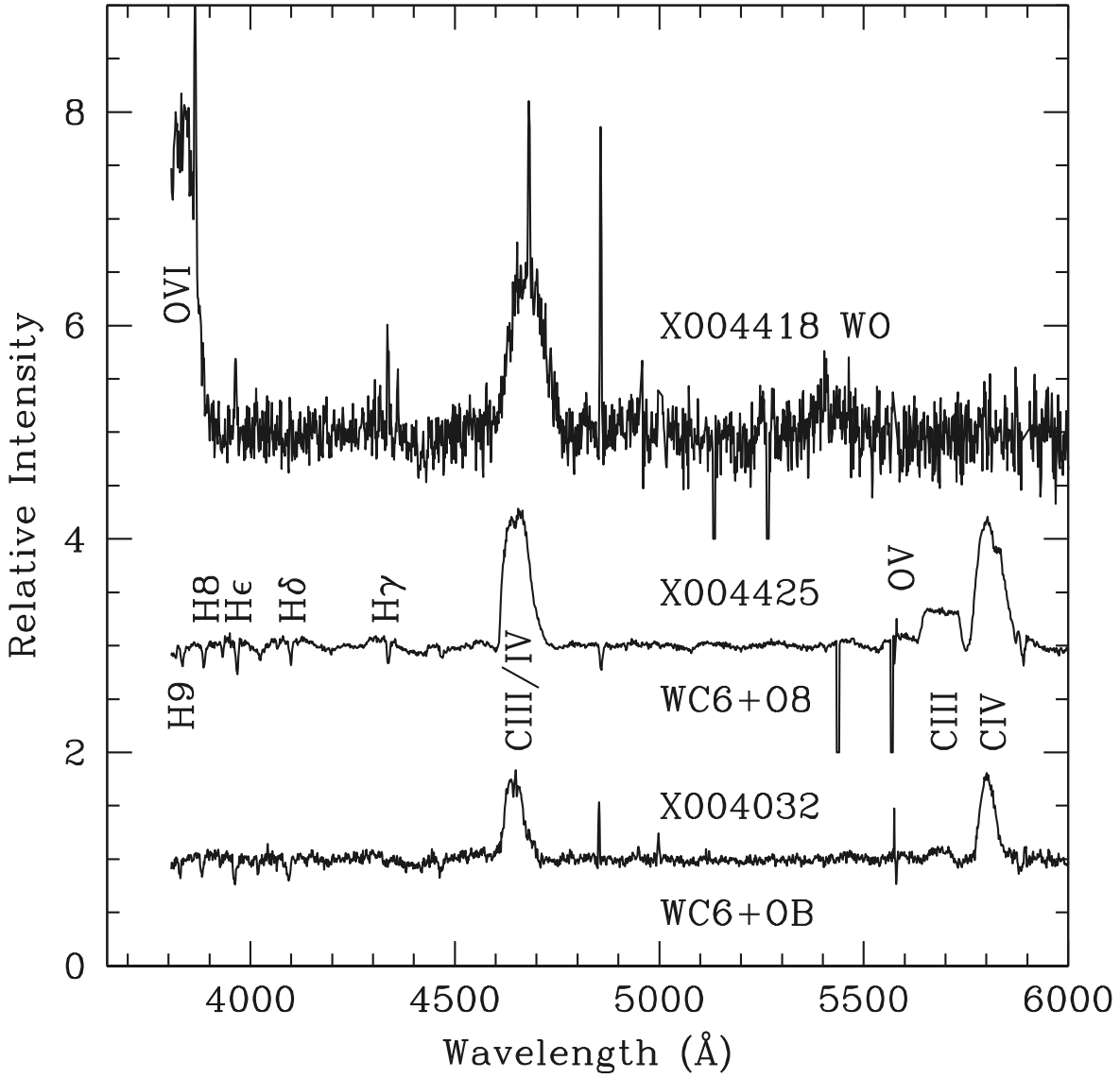

Figure 4. Spectra of representative WC/WOs. We show three example spectra of newly found WC/WO-type stars in M31. The spectra have been normalized, and only a portion of our wavelength coverage is shown for clarity. Each spectrum is offset from the previous by a relative intensity of 2.0. Lines identified include the O VI doublet $\lambda\lambda$3811, 34 (X004418.10+411850.8), the upper Balmer lines (visible in X004032.57+403901.3 and X004425.09+412046.4), the C III/IV λ4650 feature, and the classification lines O V λ5592, C III λ5696, and C IV λ5806. Note that the unnormalized version of these, and all of our spectra, are being made available in FITS format as part of this publication as "data behind figures."

gaps. For reference, the absolute magnitudes of these stars range from $M_V = -3$ for the early-type WNs up to $M_V = -6/-7$ for the late-type WNs (Crowther 2007). While the total number of stars differs by nearly a factor of 9 between the two groups, the overall subtype distribution of the newly discovered sample is similar to that of the known sample. Thus, these new stars are not intrinsically fainter as a group.

We can next examine the overall reddening of the newly discovered faint WRs. Due to their magnitudes, the majority of them are not in the LGGS (Massey et al. 2006) and thus we do not know their $B-V$ or $E(B-V)$ values. However, 61 of the previously known M31 WRs and 10 of the new WRs are within the Panchromatic Hubble Andromeda Treasury (PHAT) footprint (Dalcanton et al. 2012). Of these 10 new WRs, seven are part of the fainter sample that was missed with the previous Mosaic survey. Schlafly & Finkbeiner (2011) computed extinction values for the various ACS and WFPC3 filters. We therefore can compare the *difference* in the observed colors (e.g., F275W-F336W) between the previously known M31 WRs stars and the newly found faint sample, and compute the corresponding extra amount of reddening between the two samples. From F275W-F336W, F336W-F475W, and F475W-F814W we find very consistently that the difference in colors between the two sets corresponds to an average differences of 0.25 in $E(B-V)$, with the newly found faint sample being more highly reddened. This corresponds to roughly an additional 0.95 mag in *WN*. Therefore, these new WRs were primarily missed in our previous survey due to increased reddening causing them to be fainter than the Mosaic detection limit.

We next briefly discuss the source of this increased reddening. While WRs have high mass-loss rates (10^{-6} to 10^{-4} $M_\odot$ yr^{-1}; see Sander & Vink 2020 and references therein), this does not necessarily lead to high *local* extinction values. Overall, very few dust-enshrouded WRs have been found (see Barniske et al. 2008 for a few exceptions and an overview), though late-type WCs have been known to create

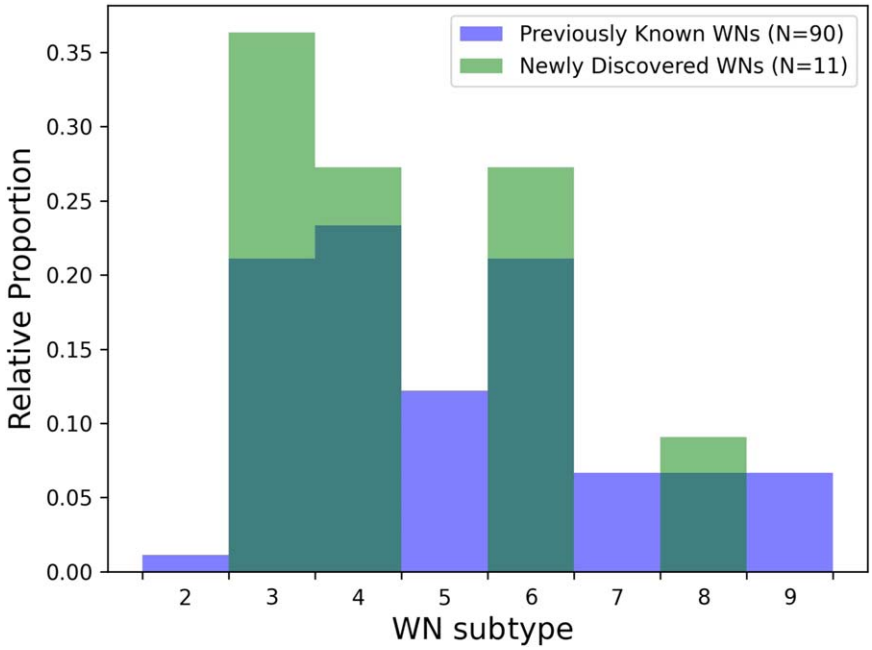

Figure 5. The relative proportion of WN subtypes compared to both the previously known and newly discovered sample of M31 WNs. While the total number of stars in each group differs, their distributions are fairly similar. This suggests that the newly discovered WRs in M31 are not predominantly part of an intrinsically fainter group of WRs.

carbon-rich dust in high-metallicity environments (Crowther et al. 2006; Williams et al. 2021). Additionally, binary WRs with highly ellipitical orbits have been observed episodically creating dust during periastron passages (see, for example, the recent images of WR140 from JWST; Lau et al. 2022). However, WRs that are heavily extincted due to their own dust seem to be the exception rather than the rule. Thus, the reddened WRs we have observed are likely located in regions of globally higher reddening due to M31's inclined orientation relative to our viewing angle.

How common are these regions of higher reddening in M31? Massey et al. (1986) investigated the massive star content of multiple OB associations in M31 using both photometry and spectroscopy. They found reddening values varying from $E(B-V) = 0.08$ (OB 102), 0.12 (NGC 206), up to 0.24 (OB 48 and the OB 8, 9, and 10 complex). They inferred that the A_V extinction of these early-type stars ranged from 0.25–0.75 mag. Massey et al. (2021b) argues that that these low numbers probably do not represent the typical extinction of the disk of M31, but rather adopts the higher $A_V \sim 1.0$ value found from PHAT data by Dalcanton et al. (2015). Wang et al. (2022) finds the same typical $A_V \sim 1.0$ value. Both Dalcanton et al. (2015) and Wang et al. (2022) argue that there are regions with much higher extinctions, but that these represent a tiny fraction (<1%) of the area of M31. As we discuss below, we hope to better quantify the reddening of these stars by obtaining new *B*, *V*, and *R* images with LMI during our upcoming observing runs. Additionally, once we have more coverage of WRs within the PHAT survey area, we can compare our results to that of M31 dust-extinction maps such as Dalcanton et al. (2015).

4.2. Did We Find the Faintest Wolf–Rayet Stars in This New Survey?

Given that our previous Mosaic survey did not go deep enough to find the faintest WRs (despite our assurances at the time; see Section 4.2 in Neugent et al. 2012), we will now reexamine this question for our current survey. Massey & Johnson (1998) emphasize that the identification of WR candidates through narrowband imaging is a line flux versus S/N issue. For instance, a bright WN star with weak He II λ4686 emission will have a small magnitude difference between the *WN* and continuum images; thus, whether or not it is detected either by photometry or by image subtraction becomes a S/N question. However, at the faint end, we can simplify the analysis by comparing the distribution of WR magnitudes through the on-band *WN* filter with the limiting magnitude of our new survey.

To determine the magnitudes of the WRs through the *WN* filter, we performed aperture photometry on all of the original Mosaic *WN* images as well as the new LMI *WN* images. The instrumental magnitudes (determined using a 3 pixel radius aperture) were then compared to the LGGS *V*-band magnitudes for all the stars categorized as being relatively uncrowded. The median differences were used to then obtain calibrated *WN* magnitudes tied to the *V*-band for all the known and newly found WRs. Results from individual images were averaged, star-by-star.

We then determined our "limiting magnitude" for both our old and new surveys. We found that on the Mosaic frames, the faintest WRs that were identified on a single dither exposure had integrated counts of about 150 ADUs (420 e-). Combining images from all three dithers resulted in a S/N ∼ 35, ignoring the minor noise contributions from read noise and sky. Thus, we defined the limiting magnitude based on photon counts corresponding to a S/N of 35, taking into account the detector gains and the number of images averaged (three for Mosaic, one or two for LMI). We find that the median limiting magnitude for our Mosaic *WN* exposures was 21.5 mag, while our LMI *WN* exposures was 23.75, a full 2.25 mag deeper. This is partially explained by the longer exposure times for the LMI data compared to Mosaic (2 × 1200 s versus 3 × 300 s), partially due to the generally better seeing (0.″9 for LMI, versus

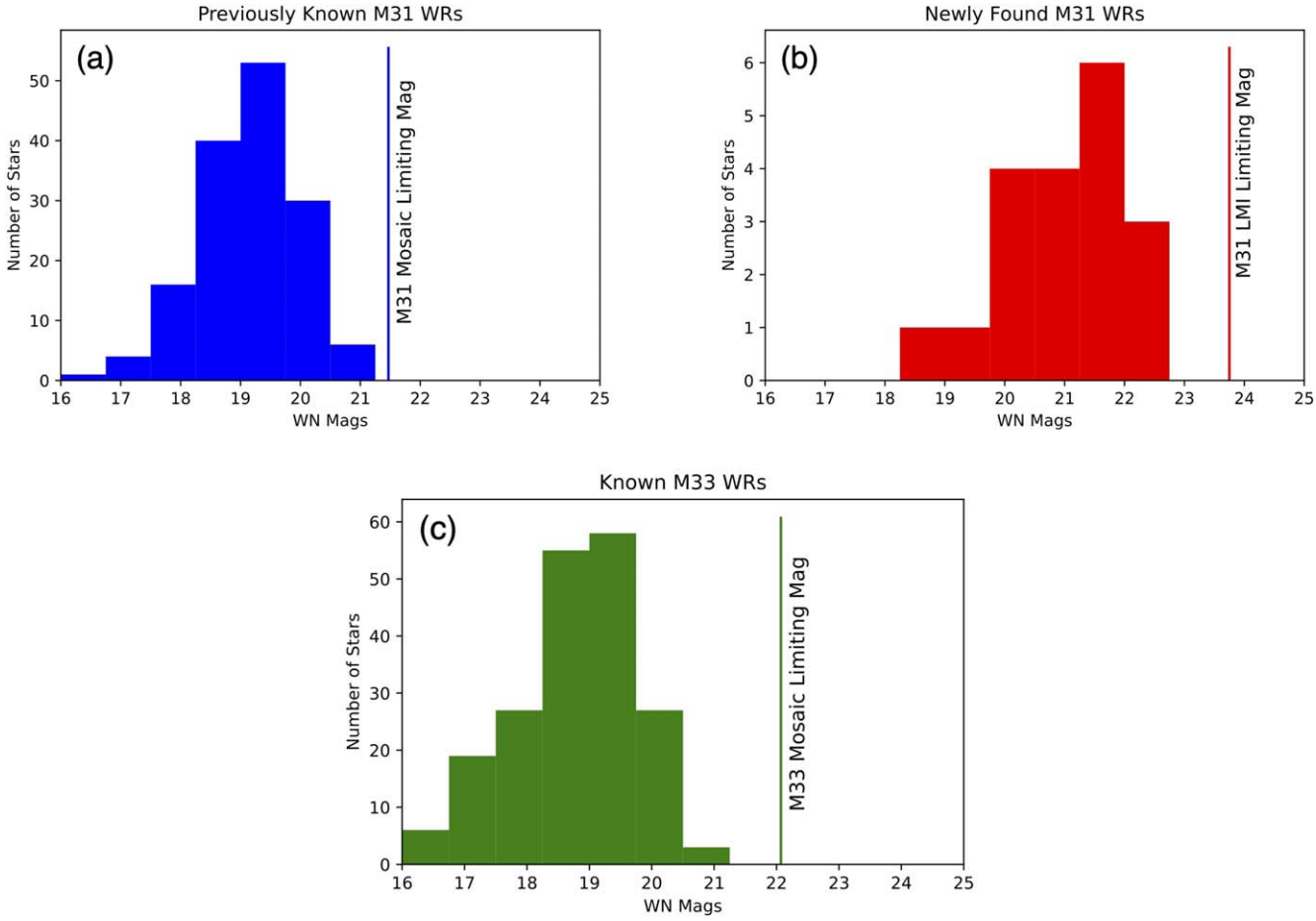

Figure 6. Distribution of *WN*-filter magnitudes of WRs in M31 and M33. The first (a) histogram shows the magnitude distribution of the previously known WRs in M31, mostly found in the Neugent et al. (2012) Mosaic camera survey. The second (b) histogram shows the distribution of the *WN* magnitudes of the newly found WRs in this survey; we have also included the magnitude we measured for the star found by Shara et al. (2016). The third (c) histogram shows the distribution of the known WRs in M33, mostly found by Neugent & Massey (2011) but also including the handful of WRs found subsequently (e.g., Neugent & Massey 2014; Massey et al. 2016). In all three histograms, the vertical line shows our estimated limiting magnitude based on a S/N of 35. The data suggest that the Mosaic M31 survey was incomplete due to sensitivity, but that our new LMI frames go deep enough. In contrast, there are unlikely to be many new WRs to be found in M33.

a median of 1.″3 for the Mosaic data), and partially to the better throughput of the LDT+LMI optical system versus that of the KPNO Mayall with the Mosaic camera.

The results are shown in panels (a) and (b) of Figure 6. It is clear from comparison of the two histograms that the newly found WRs are, for the most part, fainter than the previously known M31 WRs. Indeed, the median *WN* magnitude of the 19 newly confirmed WRs is 21.0, compared to the median *WN* magnitude of the 150 previously known WRs of 19.2. The faintest WRs in the previously known sample have a *WN* magnitude of 21.6, similar to the 21.5 mag that we estimated is the limiting magnitude of the Mosaic survey. The median *WN* magnitude of the five faintest Mosaic WRs is 21.3. In contrast, the faintest *WN* magnitude in the newly discovered sample is 23.0, and the median of the five faintest is 22.8. *These are significantly brighter than our estimated 23.75 limiting magnitude for the LMI data.*

The large gap between the magnitudes of the faintest WRs found on our LMI images and the limiting magnitude of those frames suggests that, if we had gone even deeper with the new data, we would not have discovered additional WRs in these fields. Rather, at least in these fields, we are sensitive enough to have discovered *all* of the WRs. Of course, there may be other fields in M31 where the average reddening is greater. With only 19 newly found WRs, we may also be suffering the effects of small number statistics. We plan on extending our survey to additional fields in M31 using LMI in the next observing season in order to further test this. For now, however, our analysis suggests that our newly found WRs allow us to make a meaningful estimate of the total number of WRs still to be found in M31, as we do in the next section. Furthermore, we note that our Mosaic survey needed to go about 1.5 magnitudes deeper (a factor of 4 in flux) to have reached the same limiting magnitude.

4.3. Estimating the Total Number of Wolf–Rayet Stars in M31

As part of this updated survey, we only covered ∼8% of the total optical disk of M31. If we assume that we will continue to find WRs at the same rate across the rest of the galaxy, that means we are missing almost 250 more WRs! However, as is shown in Figure 1 and discussed more extensively in Neugent et al. (2012), WRs are not evenly distributed across M31. Instead, they are generally confined to their birthplaces (dense, OB-forming regions) due to their high masses and short lifetimes. While we plan to continue our M31 survey in the upcoming observing season and answer this question conclusively, we can still place a few initial constraints on the total number of WRs we expect to find.

Overall, we found approximately the same percentage ($52\% \pm 5\%$) increase in the total number of WRs on each of the three fields we surveyed (57%, 45%, and 55%). If we assume this percentage increase will remain constant for the remaining portions of M31, we can crudely estimate that there are $\sim 80 \pm 8$ WRs missing from our previous Mosaic survey. Since we have now discovered 19 new WRs as part of this survey, there are $\sim 60 \pm 8$ more WRs left to be discovered in M31. These numbers clearly only serve as *very* broad estimates, and we look forward to constraining this number further with new observations. As mentioned previously, we purposely chose to focus this survey on areas where the Mosaic images were lacking either due to chip gaps or poor sky conditions. Therefore, this estimation for the number of missing WRs is likely a slight overestimate, rather than an underestimate.

We do note that, while the total number of WRs increased as part of our recent observing campaign, the overall ratio of WC- to WN-type WRs stayed relatively constant. As summarized in Neugent & Massey (2019), the observed ratio of WC- to WN-type WRs as a function of metallicity is an exacting test of stellar evolutionary models, and recently the observations have been in good agreement with theoretical predictions. Before discovering these new WRs, the WC/WN ratio in M31 was 0.67 ± 0.11. With the addition of 19 new WRs, the WC/WN ratio is still within the previously quoted error and is now 0.63 ± 0.10. So, while the total number of WRs has increased, the WC/WN ratio remains essentially unchanged. Additionally, although our Mosaic survey of M31 may have missed some of the fainter, more reddened stars, it was a major step foward in our knowledge of the WR content of our nearest spiral neighbor. Prior to Neugent et al. (2012), only 47 WRs were known, mostly of WC type. Their Mosaic survey added another 107, and brought the observed ratio of WC/WN stars to a value that could be compared to the evolutionary models.

4.4. What Does This Mean for M33?

As mentioned above, our discovery does raise questions about the completeness of the similar Mosaic WR survey done in M33 (Neugent & Massey 2011). Panel (c) in Figure 6 shows the distribution of the *WN* magnitudes of the M33 WRs. The limiting magnitude of the M33 Mosaic survey is significantly fainter than for the M31 Mosaic survey, 22.1 versus 21.5. The reason is easy to understand: The M33 data were taken under better conditions, with a median seeing of $1\farcs0$ rather than $1\farcs2$. The faintest WR star has a *WN* magnitude of 20.8; the median value of the faintest five WRs is 20.6 mag. These are all significantly brighter than the 22.1 mag limiting magnitude. Based on this, we do not expect there to be a significant population of missing WRs in M33. That said, we are in the process of completing a spectroscopic follow-up of M33 WR candidates found as part of a new survey with the LDT and LMI. The majority of additional candidates were located in the Mosaic gaps, but a few fainter candidates exist. We will report fully on this when the study is complete.

5. Summary and Conclusions

After several indications emerged that our previous WR survey in M31 discussed in Neugent et al. (2012) may have been incomplete (e.g., Shara et al. 2016; Massey et al. 2021a), we began a pilot survey with the goal of both finding new WRs and better understanding the completeness limits of our previous survey. The major results of this pilot survey are summarized as follows:

1. We spectroscopically confirmed 19 new WRs in M31.
2. Three of these new WRs were in the gaps of our previous survey. One of them was in the previous survey but too crowded to be readily identified. The remaining 15 new WRs were missed on the previous survey due to their faint magnitudes.
3. These 15 faint WRs are not intrinsically faint, but rather have slightly increased reddening compared to the WRs in M31 that were discovered as part of our previous survey.
4. We estimate that there are around 80 WRs missing from our previous survey, 19 of which have been discovered as part of this work. Thus, we estimate that there are around 60 WRs left to be found in M31.
5. After calculating the limiting magnitude of our new survey, and comparing it to the magnitudes of the WRs we discovered, we conclude that this new survey is not missing another even fainter population of WRs in M31.
6. We additionally conclude that our previous survey of WRs in M33 discussed in Neugent & Massey (2011) did not suffer from the same completeness issues. While there are likely a few fainter WRs left to be discovered in M33, the issue is not as severe as with M31.

We look forward to continuing this survey in the upcoming observing seasons. Besides finding new WRs, we will also obtain updated *B*, *V*, *R* photometry to better estimate the effect of reddening on our completeness limits. Our updated sample will better constrain the RSG/WR ratio discussed in Massey et al. (2021a), allow for more accurate comparisons with evolutionary models, and ultimately help us better understand the evolution and end states of massive stars.

Acknowledgments

We thank the anonymous referee for suggestions that improved the paper, as well as Ben Weiner for his assistance when designing the Binospec masks. P.M. is also grateful to his Lowell Observatory colleague Larry Wasserman for invaluable help in the astrometric refinements of the WR coordinates that enabled us to observe these stars spectroscopically with Binospec.

Additionally, we acknowledge that the work presented was done on the traditional territories and ancestral homelands of the Cheyenne, Arapaho, Ute and many other Native American nations and that Lowell Observatory sits at the base of mountains sacred to tribes throughout the region. We honor their past, present, and future generations, who have lived here for millennia and will forever call this place home.

Support for this work was provided by NASA through the NASA Hubble Fellowship grant No. HST-HF2-51516 awarded by the Space Telescope Science Institute, which is operated by the Association of Universities for Research in Astronomy, Inc., for NASA, under contract NAS5-26555. We also thank the Mt. Cuba Astronomical Foundation for their generous support, which enabled purchase of the customized interference filters used for this survey.

This research has made use of the SIMBAD database, operated at CDS, Strasbourg, France. This research has made use of the VizieR catalog access tool, CDS, Strasbourg, France

(DOI: 10.26093/cds/vizier). The original description of the VizieR service was published in A&AS 143, 23. This work has also made use of data from the European Space Agency (ESA) mission Gaia (https://www.cosmos.esa.int/gaia), processed by the Gaia Data Processing and Analysis Consortium (DPAC, https://www.cosmos.esa.int/web/gaia/dpac/consortium). Funding for the DPAC has been provided by national institutions, in particular the institutions participating in the Gaia Multilateral Agreement.

This work made use of the following facilities and software:

Facilities: LDT, MMT, Gaia.

Software: IRAF (distributed by the National Optical Astronomy Observatory, which is operated by the Association of Universities for Research in Astronomy under a cooperative agreement with the National Science Foundation), Python 3.7.4.

Appendix

The following are notes on the individual spectroscopically observed WR candidates.

J004019.66+404232.5. This is an early-type WN star with He II λ4686 and N V $\lambda\lambda$4603, 19. N IV λ4058 is also present, but weaker than the N V doublet, making this a WN3. There are strong nebular lines, primarily the [OIII] $\lambda\lambda$4959, 5007 doublet plus Balmer emission.

J004031.21+404128.1. This is a hydrogen-rich WN7 star, with N III λ4634, 42 emission about half as strong as He II λ4686. N IV λ4058 is strongly present but weaker than N IV. The even-*n* Pickering lines of He II, which are coincident with the Balmer lines, are much stronger than the odd-*n* lines, revealing the presence of hydrogen.

X004032.57+403901.3. This is a WC6 star, with C III/IV λ4650 and C IV $\lambda\lambda$5801, 12 as the strongest lines. C III λ5696 is readily visible, weaker than C IV, and O V λ5592 is weaker still. Balmer absorption from Hδ shortwards is visible, as is He I λ4471, suggesting a OB-type companion, either physical or line of sight. The fact that the C IV λ4650 line has an EW of –40 Å (rather than < -100 Å) is consistent with significant dilution by such a companion. (See the WC6 star X004054.05+403708.3, described below, with an EW of -900 Å.)

J004039.59+404449.5. Our spectrum nicely identifies this as a WN3 star, with He II λ4686, N V $\lambda\lambda$4603, 19, and N IV λ4058. The N V λ4946 line is also present.

J004042.44+404505.3. In this star N IV λ4058 and N V $\lambda\lambda$4603, 19 are the dominant nitrogen ions, with N IV of slightly greater intensity. N III $\lambda\lambda$4634, 42 is not present. Together, these comparisons lead to a WN4.5 classification. C IV $\lambda\lambda$5801, 12 is also present, although not at the intensity that would cause us to designate this a WN/C star. He II lines at 4100, 4542, 5411, and 6560 Å are all also visible with a fairly smooth progression, and there is no evidence of hydrogen.

X004045.57+404526.4. Our spectrum of this candidate shows only an inverse nebular spectrum, suggesting over-subtraction of an H II region. No continuum or WR features are evident in our spectra.

X004054.05+403708.3. The star has little continuum, but the strong C III/IV λ4650 and C IV $\lambda\lambda$5801, 12 lines stand out. C III λ5696 and O V λ5592 are of similar intensity, but with C III a bit stronger, and we thus classify this star as a WC6.

X004318.88+414711.1. This is an H II region with nebular He II λ4686 emission.

X004320.88+414107.0. This is a late-type star, with TiO bands present at 5167, 6158, and 7054 Å, probably a K7-M0. The star lacks Gaia Data Release 3 proper motions or parallaxes, but the radial velocities of the Ca II triplet in our spectrum supports membership. The star does not appear in Table 2 of Massey et al. (2023), presumably as it is too faint.

J004326.06+414260.0. The star shows N V $\lambda\lambda$4603, 19 with comparable N IV λ4058, but no N III $\lambda\lambda$4634, 42. Thus, we classify it as WN4. There are strong He II lines, but a smooth progression from even-*n* to odd-*n*, giving no evidence of hydrogen. A strong nebular spectrum is also present. C IV $\lambda\lambda$5801, 12 is also present, but again not at a level such that we would call this a WN/C.

X004332.04+414817.2. This is an H II region with nebular 4686 Å emission.

X004338.95+414327.0. The spectrum is dominated by nebular emission, but there is clearly a broad component at 4686 Å. The star is of WN type but we cannot classify it more exactly.

X004341.15+414413.6. Our two spectra of this star are compromised by a strong oversubtraction near the 4650-4686 Å complex, some sort of reduction issue. Nevertheless, we can classify this as a late-type WN, with N III $\lambda\lambda$4634, 42 equal in intensity to He II λ4686. The star is clearly of WN type rather than an Of-type star, as He I λ5876. Hα is also present in emission. C IV $\lambda\lambda$5801, 12 is as strong as He II λ4686, and so we call this an WN8/C star.

X004353.03+412141.0. This is a late-type WC, as evidenced both by the fact that C III λ5696 is comparable in strength to C IV $\lambda\lambda$5801, 12, and the fact that the lines are relatively skinny for a WC. We classify this as a WC7. Both the line fluxes and the continuum are weak; with a less powerful instrument or shorter exposure times, this star would not have been detected as a WR. A strong nebular spectrum is also present.

X004359.44+414823.9. We classify this as a WN6, as N III $\lambda\lambda$4634, 42 is about the same intensity as N IV λ4058, with N V $\lambda\lambda$4603, 19 weakly present. He II emission is weakly present.

J004404.10+411710.5. This is an H II region but without He II λ4686 emission. It is not clear why this star was selected as a WR candidate.

X004406.41+412020.8. N IV λ4058 and N V $\lambda\lambda$4603, 19 are the dominant nitrogen ions in this WN star, with N III $\lambda\lambda$4634, 42 very weakly present. N IV is slightly stronger than N III, We therefore classify this as a WN4.5. There is no odd-*n*, even-*n* discrepancies among the Pickering lines, and so the star shows no obvious evidence of hydrogen. C IV $\lambda\lambda$5801, 12 is weakly present.

J004408.13+412100.6. The lines are sharp and strong in this late-type WN star. N IV λ4058 is the dominant nitrogen ion, but in similar intensity to N III $\lambda\lambda$4634, 42, with N V $\lambda\lambda$4603, 19 quite visible but much weaker, leading to a WN4.5 classification. Strong nebular lines are present.

J004413.56+412004.7. This is another WN4.5 star, with N IV λ4058 marginally stronger than N V $\lambda\lambda$4603, 19 and N III $\lambda\lambda$4634, 42 absent. The He II emission sequence does not suggest the presence of hydrogen.

X004414.71+414033.3. This is an interesting but odd discovery. The object is not a WR star, but narrow, nebular-like emission is present at He II λ4686 as well as Hα, Hβ, Hγ, and Hδ. However, the expected forbidden lines of O [III] $\lambda\lambda$4959, 5007 are not present. TiO band absorption at 5167, 6158, and 7054 Å and a red continuum suggests an

underlying M0-ish star present. We believe this is a symbiotic star. There is also strong emission present at a rest wavelength of 5583 ± 1 Å, which we were unable to identify.

X004418.10+411850.8. There are only two WR features present in our spectrum, broad C III/IV λ4650 and O VI $\lambda\lambda$3811, 34. The latter is even stronger than the C III/IV, making this star a WO type. No WR lines are visible in the yellow in our spectrum, and so we cannot give a more exact subtype. Strong nebular emission is seen.

X004421.30+411807.2. The star appears to be of Of type, with N III $\lambda\lambda$4634, 42 and He II λ4686. The EW of the latter is -4 Å. The pipeline reduction has oversubtracted nebular emission, but He I λ4387 and λ4471 absorption are present, as well as He II λ4200 and λ4542 absorption, in addition to Balmer absorption. We classify the star as O6 If.

X004423.98+412255.6. This is a cool star, with TiO bands at 5167, 5847, 6158, 6658, and 7054 Å. The presence of the 5847 and 6658 Å suggests a spectral subtype later than M0, probably more like an M2. There are no Gaia data for this star, but an examination of the the Ca II triplet shows a radial velocity consistent with M31 membership. The star is not included in Table 2 of Massey et al. (2023), presumably because it is too faint.

X004425.09+412046.4. This is a classical WC6 emission spectrum on a strong continuum with O-type absorption lines at shorter wavelengths. We tentatively classify the companion as O8.

X004426.99+411928.0. There is a relatively early-type absorption present, but with no sign of He I or He II. There is no He II λ4686. This star was included as a WR candidate likely because it was too bright for image subtraction to work correctly (see discussion in Section 2.1.2).

X004431.39+412114.0. N V $\lambda\lambda$4603, 19 is the dominant nitrogen line in this star, with very weak N III $\lambda\lambda$4634, 42 present. No N IV λ4058 is visible but the spectrum is very noisy in the far blue. We classify this star as a WN3. A strong nebular spectrum is also present.

X004432.06+411940.5. This is an H II region with He II λ4686 emission. There is also an absorption line spectrum present, mainly evidenced in the upper Balmer region.

J004433.91+412501.2. N IV λ4058, N V $\lambda\lambda$4603, 19, and N III $\lambda\lambda$4634, 42 are all present in our spectrum of this star, with N IV the strongest and N V the weakest. We call this a WN6 type. C IV $\lambda\lambda$5801, 12 is also present at modest intensity. Strong nebular lines are present.

X004438.04+412518.7. The spectrum of this star is very similar to that of J004433.91+412501.2, except no C IV is evident. We classify this as a WN6.

X004440.49+412052.1. This is another H II region with He II λ4686 emission.

ORCID iDs

Kathryn F. Neugent https://orcid.org/0000-0002-5787-138X
Philip Massey https://orcid.org/0000-0001-6563-7828

References

Aadland, E., Massey, P., Hillier, D. J., et al. 2022, ApJ, 931, 157
Abbott, B. P., Abbott, R., Abbott, T. D., et al. 2016, PhRvL, 116, 061102
Armandroff, T. E., & Massey, P. 1985, ApJ, 291, 685
Barniske, A., Oskinova, L. M., & Hamann, W. R. 2008, A&A, 486, 971
Bartzakos, P., Moffat, A. F. J., & Niemela, V. S. 2001, MNRAS, 324, 18
Becker, A. 2015, HOTPANTS: High Order Transform of PSF ANd Template Subtraction, Astrophysics Source Code Library, ascl:1504.004
Bhattacharya, S., Arnaboldi, M., Hartke, J., et al. 2019, A&A, 624, A132
Bida, T. A., Dunham, E. W., Nye, R. A., Chylek, T., & Oliver, R. C. 2012, Proc. SPIE, 8444, 844451
Cassinelli, J. P., & Hartmann, L. 1975, ApJ, 202, 718
Ciardullo, R., Jacoby, G. H., Ford, H. C., & Neill, J. D. 1989, ApJ, 339, 53
Conti, P. S. 1978, ARA&A, 16, 371
Conti, P. S., Leep, M. E., & Perry, D. N. 1983, ApJ, 268, 228
Conti, P. S., & Massey, P. 1989, ApJ, 337, 251
Cox, A. N. 2000, Allen's Astrophysical Quantities (New York: Springer)
Crowther, P. A. 2007, ARA&A, 45, 177
Crowther, P. A., Morris, P. W., & Smith, J. D. 2006, ApJ, 636, 1033
Dalcanton, J. J., Fouesneau, M., Hogg, D. W., et al. 2015, ApJ, 814, 3
Dalcanton, J. J., Williams, B. F., Lang, D., et al. 2012, ApJS, 200, 18
DeGroff, W. T., Levine, S. E., Bida, T. A., et al. 2014, Proc. SPIE, 9145, 91452C
Dorn-Wallenstein, T. Z., & Levesque, E. M. 2018, ApJ, 867, 125
Dsilva, K., Shenar, T., Sana, H., & Marchant, P. 2022, A&A, 664, A93
Eldridge, J. J., Stanway, E. R., Xiao, L., et al. 2017, PASA, 34, e058
Fabricant, D., Fata, R., Epps, H., et al. 2019, PASP, 131, 075004
Foellmi, C., Moffat, A. F. J., & Guerrero, M. A. 2003, MNRAS, 338, 1025
Gaia Collaboration, Brown, A. G. A., Vallenari, A., et al. 2018, A&A, 616, A1
Gaia Collaboration, Brown, A. G. A., Vallenari, A., et al. 2021, A&A, 649, A1
Hainich, R., Pasemann, D., Todt, H., et al. 2015, A&A, 581, A21
Hamann, W. R., Koesterke, L., & Wessolowski, U. 1995, A&AS, 113, 459
Hillier, D. J., Aadland, E., Massey, P., & Morrell, N. 2021, MNRAS, 503, 2726
Kansky, J., Chilingarian, I., Fabricant, D., et al. 2019, PASP, 131, 075005
Lang, D., Hogg, D. W., Mierle, K., Blanton, M., & Roweis, S. 2010, AJ, 139, 1782
Lau, R. M., Hankins, M. J., Han, Y., et al. 2022, NatAs, 6, 1308
Levine, S. E., Zuluaga, C. A., Person, M. J., et al. 2021, AJ, 161, 210
Massey, P., Armandroff, T. E., & Conti, P. S. 1986, AJ, 92, 1303
Massey, P., & Johnson, O. 1998, ApJ, 505, 793
Massey, P., Neugent, K. F., Dorn-Wallenstein, T. Z., et al. 2021a, ApJ, 922, 177
Massey, P., Neugent, K. F., Ekström, S., Georgy, C., & Meynet, G. 2023, ApJ, 942, 69
Massey, P., Neugent, K. F., Levesque, E. M., Drout, M. R., & Courteau, S. 2021b, AJ, 161, 79
Massey, P., Neugent, K. F., & Morrell, N. 2015, ApJ, 807, 81
Massey, P., Neugent, K. F., & Morrell, N. 2017, ApJ, 837, 122
Massey, P., Neugent, K. F., Morrell, N., & Hillier, D. J. 2014, ApJ, 788, 83
Massey, P., Neugent, K. F., & Smart, B. M. 2016, AJ, 152, 62
Massey, P., Olsen, K. A. G., Hodge, P. W., et al. 2006, AJ, 131, 2478
Merrett, H. R., Merrifield, M. R., Douglas, N. G., et al. 2006, MNRAS, 369, 120
Moffat, A. F. J., & Shara, M. M. 1983, ApJ, 273, 544
Neugent, K., & Massey, P. 2019, Galax, 7, 74
Neugent, K. F., & Massey, P. 2011, ApJ, 733, 123
Neugent, K. F., & Massey, P. 2014, ApJ, 789, 10
Neugent, K. F., Massey, P., & Georgy, C. 2012, ApJ, 759, 11
Neugent, K. F., Massey, P., & Morrell, N. 2018, ApJ, 863, 181
Sander, A. A. C., & Vink, J. S. 2020, MNRAS, 499, 873
Santana-Ros, T., Micheli, M., Faggioli, L., et al. 2022, NatCo, 13, 447
Schlafly, E. F., & Finkbeiner, D. P. 2011, ApJ, 737, 103
Schnurr, O., Moffat, A. F. J., St-Louis, N., Morrell, N. I., & Guerrero, M. A. 2008, MNRAS, 389, 806
Shara, M. M., Mikołajewska, J., Caldwell, N., et al. 2016, MNRAS, 455, 3453
Shenar, T., Hainich, R., Todt, H., et al. 2016, A&A, 591, A22
Shenar, T., Sablowski, D. P., Hainich, R., et al. 2020, A&A, 641, C2
Stetson, P. B. 1987, PASP, 99, 191
Torres-Dodgen, A. V., & Massey, P. 1988, AJ, 96, 1076
van der Hucht, K. A. 2001, NewAR, 45, 135
Wang, Y., Gao, J., & Ren, Y. 2022, ApJS, 259, 12
Williams, P. M., Morrell, N. I., Boutsia, K., & Massey, P. 2021, MNRAS, 505, 5029
Woosley, S. E., Sukhbold, T., & Janka, H. T. 2020, ApJ, 896, 56
Wray, J. D., & Corso, G. J. 1972, ApJ, 172, 577